Journal of Physics: Conference Series **3124** (2025) 012006 doi:10.1088/1742-6596/3124/1/012006

External electron injection setup for the advanced wakefield experiment (AWAKE) run 2b

N Z van Gils[1,2], M Turner[2], G Zevi Della Porta[2,4], F Pannell[3], V Bencini[2,5], A Gerbershagen[1] and E Gschwendtner[2] for the AWAKE Collaboration

[1] PARTREC, UMCG, University of Groningen, Groningen, NL
[2] CERN, Geneva, CH
[3] University College London, London, UK
[4] Max Planck Institute for Physics, Munich, DE
[5] John Adams Institute for Accelerator Science, University of Oxford, Oxford, UK

E-mail: nikita.zena.van.gils@cern.ch

Abstract. AWAKE is a plasma wakefield acceleration R&D experiment at CERN, where wakefields are driven by relativistic and self-modulated proton bunches. The goal of AWAKE Run 2b is to demonstrate that a correctly placed plasma density step stabilises the wakefield amplitude (after saturation of self-modulation) at a higher value than without the step. This can be demonstrated by accelerating witness particles. It is therefore planned to externally side-inject 19 MeV test electrons into the wakefields. In this manuscript, the injection setup for the AWAKE Run 2b experiments is summarised. Challenges on beam transport due to the Earth's magnetic field upstream of the vapour source entrance are highlighted and uncertainties on the injection location are estimated. Additionally, a new plasma-light-based diagnostic to verify that electrons cross the plasma column is introduced.

1. Introduction

Plasma wakefield acceleration is a promising concept to accelerate charged particles with gradients exceeding GeV/m. These gradients are several orders of magnitude higher than those achievable in radio-frequency cavities ($<\sim$200 MeV/m).

Plasma wakefields can be excited by charged particle bunches or laser pulses. When they propagate through a plasma, their space-charge or ponderomotive force generates charge separation between plasma electrons and ions. This charge separation sustains fields, also called wakefields. Wakefields have transverse and longitudinal components, which allow to focus and accelerate trailing witness bunches.

In the linear regime, wakefields are sinusoidal with a periodicity of the plasma electron wavelength $\lambda_{pe} = 2\pi c/\omega_{pe}$, with $\omega_{pe} = \sqrt{\frac{n_{pe}e^2}{\epsilon_0 m_e}}$ the plasma electron frequency, c the speed of light, m_e the electron mass, e the electron charge, ϵ_0 the vacuum permittivity and n_{pe} the plasma electron density. One quarter of the wakefield period can be used to accelerate and focus a charged witness bunch.

For effective acceleration in wakefields, a witness bunch must stay in the focusing and accelerating phase over the entire plasma. That is the case when the phase slippage between the driver and wakefield is smaller than $\sim \lambda_{pe}/4$. If the witness bunch enters the focusing

and decelerating wakefield phase, the energy gain is reduced. If it enters the defocusing and accelerating phase, the bunch is lost due to defocusing.

There are several reasons why witness bunches may dephase in the wakefields. For example, the driver group velocity v_{ph} may be significantly smaller than the velocity of the witness bunch (typically close to c). Another example is an evolution of v_{ph} during the development of self-modulation. In that case, witness bunches need to be injected after or close to saturation of the instability, where v_{ph} becomes equal to the velocity of the drive bunch train.

In this manuscript, the technical realisation of the witness injection setup for the Advanced Wakefield Experiment (AWAKE) Run 2b experiment is presented. The setup is meant to inject electrons at a certain distance z_e into the plasma to avoid dephasing between electrons and wakefields. Challenges are highlighted with a focus on upgrades implemented since AWAKE Run 1 (2016-2018) [1]. In particular, the proof-of-principle results are presented, showing that a plasma-light-based diagnostic may be used to experimentally determine where witness electrons are injected.

The manuscript is structured as follows. In Section 2, the AWAKE experiment and its new vapour source setup with the possibility of a density step in plasma is introduced. In Section 3, the witness bunch transport to the vapour source entrance as well as the injection configuration is described. In Section 4, alignment challenges and witness beam optics are discussed. Finally, in Section 5, an estimate on the uncertainty of the witness injection location is made and the novel plasma-light-based diagnostic is introduced.

2. The AWAKE experiment

AWAKE is an R&D experiment at CERN aiming to develop proton-driven plasma wakefield acceleration. Wakefields are driven by highly relativistic (400 GeV, relativistic factor $\gamma_{p+} \sim 427$) and energetic (>19 kJ) proton bunches supplied by the CERN Super Proton Synchrotron (SPS). Due to unavailability of short ($< \lambda_{pe}$) and dense ($\sim n_{pe}$) bunches, bunches have to be self-modulated to excite wakefields with GV/m amplitudes [2, 3].

AWAKE uses plasma densities between 10^{14} and 10^{15} cm^{-3} (corresponding to $\lambda_{pe} \sim 3{-}1$ mm). The plasma is created by laser ionization (pulse length: $\sim$ 120 fs, energy per pulse: $\sim$ 100 mJ, central wavelength: 780 μm) of rubidium vapour [4, 5]. It is 10 m long, with a radius of $\sim$ 1 mm. The laser pulse additionally creates a relativistic ionization front that can serve as the seed for the self-modulation process [6, 7].

During AWAKE Run 1 (2016-2018), the successful development of seeded self-modulation of the proton bunch and subsequent wakefield growth were demonstrated [8, 9]. Externally injected $\sim$ 19 MeV electrons were accelerated up to 1.5 GeV in a uniform 10 m-long plasma and up to 2 GeV when adding a 2 % density gradient over the 10 m [10].

Simulation studies confirm that the addition of a plasma density gradient leads to higher average wakefield amplitudes than a plasma without a gradient [11]. They also show that the use of a plasma density step (during the development of self-modulation) allows to stabilise field amplitudes at high values after saturation of self-modulation. Demonstrating that a plasma density step stabilises the wakefield amplitude at high values is the goal of the AWAKE Run 2b experiment [12].

To realize these experiments, a new vapour source was developed and installed [13]. This source allows to add a 0-9 % density step between 0.25 m and 4.25 m (in intervals of 0.5 m) to an otherwise uniform density profile. A schematic drawing of the vapour source is included on Fig. 1.

Due to the complexity of the vapour source, there is currently no beam diagnostic inside the source. However, there are ten equally spaced view-ports (between 0.5 and 9.5 m). These are equipped with digital cameras imaging the vapour source center. In Sec. 5.2 it is detailed how these cameras are used to image the light emitted by the plasma.

3. Setup for the AWAKE Run 2b witness injection

3.1. Witness bunch production and transport

The electron witness bunch is produced by a photo-injector. Electrons are extracted from a Cs_2Te cathode by a UV laser pulse (typical spot size: ~ 1 mm, average energy: 200 nJ, top hat intensity profile). First, an S-band RF-photo-injector [14] accelerates them to an energy of ~ 5 MeV. After that, they are accelerated to ~ 19 MeV in a 1 m-long booster structure [15, 16].

The final bunch length is $\sim 2-5$ ps and therefore comparable to the plasma wavelength for the nominal AWAKE plasma density ($n_{pe} = 7 \times 10^{14}\,\mathrm{cm}^{-3}$ and $\lambda_{pe}/c = 4$ ps). These long bunches facilitate temporal alignment as some part of the witness bunch always overlaps with the accelerating and focusing wakefield phase.

The charge per bunch is varied by changing the UV laser pulse illumination area. Typical bunch charges are between 100 and 800 pC, as measured using a Faraday cup. Typical normalised emittance values range between 1 and 3 mm·mrad (depending on the bunch charge), measured using quadrupole scans.

Witness bunches are transported to the vapour source entrance using a 15 m-long transport line [18]. Due to the use of linear optical elements (dipoles and quadrupoles) in the transport line, emittance preservation is assumed during transport to the vapour source entrance. However, dispersion reaches significant values along the line, especially in the horizontal plane [18]. This explains the asymmetric shape of the measured beams prior to the vapour source for focal points inside the vapour source. The optics are designed to minimise dispersion at focus. The transverse beam distributions have tails. These tails and non-linear features in the transverse beam distribution come from the injector [15, 17].

For focusing, two quadrupole triplets are used. The focal point location can be varied from several meters upstream of the vapour source entrance to the vapour source exit. This flexibility in the focal point location allows to optimize charge capture in the wakefields, by increasing the charge density at the injection location. More discussion on the injection configuration is provided in Section 3.2.

The beam transport line includes beam screen systems (BTVs) that are used to measure transverse, time-integrated bunch profiles. The BTV screens are thick enough to stop (or significantly scatter) the electron bunch. Therefore one can only perform measurements at one location at a time. In addition, there are eleven beam position monitors (BPMs). These are non-invasive and continuously provide the electron bunch centroid position along the beamline. More details on the electron beam diagnostics can be found in [19].

3.2. External, off-axis injection

AWAKE requires external injection of the electron witness bunch. This is because wakefields are of relatively low amplitude ($\sim$0.5 GV/m) and high phase velocity (relativistic factor $\gamma \sim \gamma_{p^+} \sim 427$)[20, 21]. Electrons can be captured when 1) they overlap with the focusing and accelerating plasma wakefield phase (spatially and temporally) and 2) their initial velocity is close to v_{ph}. For AWAKE parameters, the injected bunch energy must exceed $\sim$1.5 MeV [1]. The injection energy of ~ 19 MeV is therefore sufficient.

Due to the development of the proton bunch during self-modulation, the wakefield phase velocity (v_{ph}) evolves significantly over the first few meters of plasma. Additionally, initial adiabatic wakefields (driven by the proton bunch, before self-modulation) defocus the low energy electron bunch. To avoid losing the witness bunch, injection is performed at a location z_e, after v_{ph} has stabilised (typical z_e $\sim$2-4 m). To realise that, injection is performed off-axis (see Fig. 1).

As indicated on Fig. 1, part of the electron beam line is common with the proton beam line. While there are no proton beam corrector magnets, there are several electron beam corrector magnets. These have a low enough field strength and length product to have a negligible effect on the significantly more rigid proton beam. The last two electron beam corrector magnets

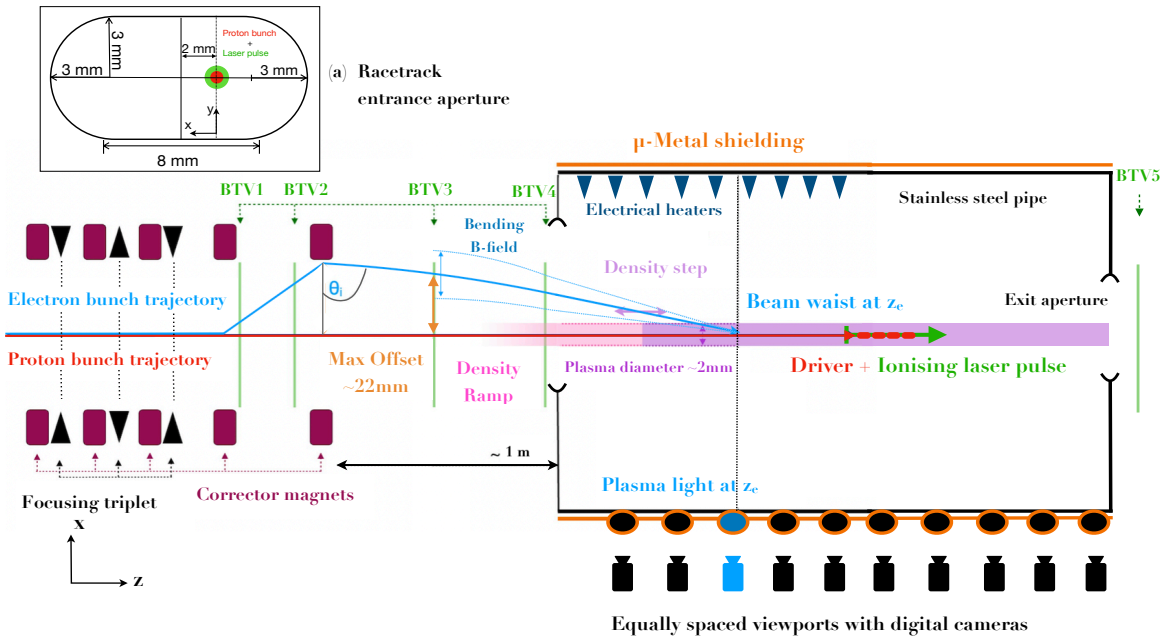

Figure 1. Schematic drawing illustrating proton (red) and electron (light blue) bunch trajectories (including bending by Earth's B-field). The entrance of the vapour source (racetrack aperture) is defined as $z = 0$. Inside the vapour source (black), the self-modulated driver (red) and ionising laser pulse (green arrow) are illustrated. Also shown are BTVs including the first one after the (circular of radius 5 mm) vapour source exit. Corrector magnets (defining trajectory) and the last quadrupole triplet of the electron beam line are indicated. On one side of the vapour source view-ports (illustrated only unilaterally), digital cameras are installed. Highlighted (lightblue), the camera at injection position z_e. Illustrated only on one side (dark blue), are the electrical heaters. The μ-metal encasing (orange) shields the vapour source from external magnetic field. Top left (a), vapour source entrance aperture and its dimensions. The green circle indicates the full width half maximum (FWHM) transverse size of the laser pulse. The red circle indicates the three sigma envelope of the transverse proton bunch distribution. Drawings are not to scale.

(henceforth referred to as corrector magnets due to their negligible effect on the magnetically rigid proton beam), the last of which is located 1.027 m away from the entrance aperture, are used to align and set the entrance angle θ_i into the vapour source and thus the location of injection, z_e, of the witness bunch, see Section 3.2.1. Simulation results suggest that injection angles $>\theta_i \sim 1$ mrad are required to capture electrons in the wakefields, and that larger θ_i, up to a few milli-radians are favoured [22, 23].

During operation, alignment checks are performed using the last two BTVs prior to the entrance aperture (BTV3 and BTV4 in Fig. 1). These are located 0.802 m and 0.091 m upstream of the entrance aperture.

The BPMs on the shared beam line (last one located 2 m upstream of the entrance aperture, not shown on Fig. 1) are unable to measure the electron bunch position in the presence of

the proton bunch since the proton bunch signal (large population 3×10^{11} protons per bunch) dominates over the electron bunch signal ($(0.6 - 3.6) \times 10^9$ electrons per bunch). BPMs that will allow measurement of the electron bunch position in the presence of the proton bunch are under development for AWAKE Run 2c [24].

Beam steering challenges due to the Earth's magnetic field will be discussed in Section 4.1. Limits on the injection angle into the wakefields and offset will be estimated in the next Section.

3.2.1. Vapour source entrance aperture and limits on the injection angle

The vapour source that was used for the AWAKE Run 1 experiments had a circular entrance aperture (radius 5 mm). This aperture was limiting the entrance and equal injection angle θ_i, when assuming a straight line trajectory.

For the new vapour source (see Section 2), the aperture was changed to be horizontally elongated. This aperture has a racetrack shape (see Fig. 1a) to allow for larger horizontal injection angles (θ_i). While the shape changed, the area of the entrance aperture was kept the same as the exit aperture, in order to keep rubidium flow to the expansion volume at a similar level [25]. The geometric center of the aperture is horizontally offset by 2 mm and allows for up to Δx_a =9 mm offset between electron and proton bunches at the entrance aperture. Horizontal elongation and offset were chosen because the electron bunch transverse distribution (for most focal positions) is horizontally elongated due to dispersion in the transport line.

Horizontally elongated electron beam shapes together with the aperture limitations allow to estimate the maximum injection angle $\theta_{i,max}$. The maximum offset (with respect to the proton bunch trajectory) at the location of BTV2 is limited by the BTV screen size and is Δx_{BTV3} =22 mm. The maximum offset at the entrance aperture is Δx_a =9 mm (see Fig. 1).

Let z_e be a desired crossing point between the electron and proton bunch (wakefields). Furthermore, assume the electron bunch waist to be located at z_e. For example z_e =2 m would imply that the electron bunch is focused at *and* crosses the wakefields 2 m downstream of the vapour source entrance. For a straight line trajectory of the electron bunch, from BTV3, inside the vapour source, to the location of injection, by similarity of triangles, the geometry and offset of the aperture allows for a maximum entrance and injection angle:

$$\theta_{i,max} = \min\{\frac{\Delta x_{BTV3} - 2\sigma_{x,BTV3}}{z_e + d_{BTV3,a}}, \frac{\Delta x_a - 2\sigma_{x,a}}{z_e}\}, \tag{1}$$

where $d_{BTV3,a} = 1.027$ m is the distance between BTV3 and the entrance aperture and $\sigma_{x,BTV3}$ and $\sigma_{x,a}$ are the horizontal beam sizes at BTV3 and the entrance aperture, respectively. Equation (1) assumes no limitations in the vertical axis and the electron beam is assumed to be aligned on the proton beam trajectory. A 2σ beam envelope is chosen, to keep electron bunch losses low.

Equation (1) shows that $\theta_{i,max}$ is either limited by the horizontal offset Δx_{BTV3} on BTV3 (left term in Eq. (1), or the entrance aperture dimensions of the vapour source (right term in Eq. (1). If z_e is close to or at the vapour source entrance, the horizontal offset on BTV3 limits $\theta_{i,max}$. If a z_e further downstream the vapour source entrance is chosen, the transverse electron bunch size at the aperture $\sigma_{x,a}$ becomes large and limits $\theta_{i,max}$. The larger z_e, the smaller $\theta_{i,max}$, because of the increase of $\sigma_{x,a}$ as $\sigma_{x,a} = \sigma_w\sqrt{1 + (z_e/\beta^*)^2}$, where σ_w is the electron beam transverse size at the waist and β^* is the electron beam beta function at the waist.

4. Electron beam transport challenges

Ideally, particle beam transport is determined by the magnetic elements of the beam line, where magnetic dipoles define beam trajectory and quadrupoles beam envelope. Within our measurement accuracy, this was observed to be the case for the 400 GeV proton beam line

used in the AWAKE experiment. However, a significant deviation from the expected straight line trajectory was noticed when using the ∼19 MeV electron beam. The low beam energy (and therefore low magnetic rigidity) leads to significant trajectory alteration in the presence of relatively weak magnetic fields, e.g. the Earth's magnetic field or any fields originating from surrounding equipment, e.g. vapour source heaters.

To minimize external magnetic fields and their influence, the entire vapour source is encased in magnetic field shielding μ-metal. However, due to the many magnetic, and beam diagnostics elements, the electron beam transport line could not be shielded. As a result, magnetic field effects from various contributions along the electron transport line, as described below, must be accounted for.

4.1. Earth's magnetic field

During operation of the electron beam line, it was experimentally observed that the electron beam trajectory is bent compared to the proton beam trajectory. The observed deviations are consistent with the presence of a large-scale, constant magnetic field, causing a deflection in the horizontal and vertical planes. Deviations are measurable at different points along the electron beam line and were not observed to change over the time scale of several weeks.

Earth's magnetic field measurements [26] showed strengths of $B_x = 0.04\,\mathrm{mT}$ and $B_y = 0.02\,\mathrm{mT}$ in 2017 in the AWAKE tunnel [27]. Magnetic fields of that order cause millimeter scale displacements over meter-scale distances for the ∼19 MeV electron bunch. For example a field strength of ∼0.04 mT results in a bending (Larmor) radius of ∼1.5 km. The electron beam trajectory is assumed circular in both planes (x and y), as opposed to helical. The electron beam momentum is strongest in z, thus it will interact with the x and y magnetic field components. Once the electron beam gets bent and acquires momenta in x and y, it interacts with the magnetic field in z (which if assumed of comparable magnitude to the fields in x and y would lead to significant deflections of the electron beam in x and y). Given the small deflections measured in x and y [26], the effect of the magnetic field in z is assumed comparatively small.

Surrounding equipment (e.g. vapour source heaters, diagnostics, magnets) is frequently switched on and off or its current is varied. It is therefore hypothesised that the most significant electron trajectory bending effect prior to the entrance aperture is associated with the external, static Earth's magnetic field, as thoroughly described in [27].

The electron beam bending radius was experimentally evaluated by measuring the beam centroid position on three BTVs (BTVs 2, 3 and 4, located 1.25 m, 0.802 m and 0.09 m upstream of the vapour source entrance). Three measurement points allow to unambiguously define the circular trajectory.

For these measurements, the electron beam waist is placed at BTV3, to minimize beam sizes on the BTVs$2-4$, which facilitates centroid determination. Beam centroid positions are obtained from Gaussian fits to the projections of the measured time-integrated bunch density distributions. A measurement example for centroid determination is shown in Fig. 2 and discussed in Section 4.3.

There are no quadrupoles between the aforementioned measurement points. However, there are corrector magnets in close proximity; the last corrector used for alignment of the electron beam, for example, is between the first two of these measuring points. In order to minimise remnant fields and potential effects on the electron beam trajectory, these magnetic elements are de-gaussed and their current is set to zero prior to starting the measurement. Additionally, the measurement was repeated using a fourth BTV further upstream (BTV1, with different electron beam optics, setting the waist at BTV2, to minimize transverse beam sizes on the screens and simplify centroid determination). The measurements support the assumption of a constant effect along the last $\sim 4\,\mathrm{m}$ of the shared beam line, and obtain the same values of bending radius, within the uncertainty of the measurements.

In order to measure deviations from a straight line trajectory, a zero reference is required; ideally, this would be obtained from a laser pulse. However, the only laser pulse available has a large spot size and centroid determination is thus inaccurate.

As an alternative the 400 GeV proton beam is used. It has a relatively small transverse size ($\sim$ 165 μm measured on BTV4 when focused at the vapour source entrance), a transversely Gaussian profile and can be measured on all beam screens simultaneously. Furthermore, by comparing the momentum of the proton ($\gamma_{p+}m_{p+}$) and electron bunch ($\gamma_e m_e$), where $\gamma_{p+,e}$ is the relativistic gamma factor and $m_{p+,e}$ the rest mass of the proton and electron bunch respectively, the effect of the Earth's magnetic field on the proton bunch, compared to the electron bunch, is smaller by a factor of 2.6×10^4. This validates the assumption of a (relative) straight line trajectory of the proton bunch [26]. As a result, the horizontal and vertical electron beam centroid positions, with respect to that of the proton beam centroid, are measured. An example for centroid determination of an imaged beam on BTV4 is shown in Fig. 2, the focus is at the entrance aperture, ~ 0.09 m further in the positive z-direction.

When placing the beam waist in the middle of the three BTVs (BTV3), one obtains values for the horizontal and vertical radius of curvature, $R_x = (2800 \pm 700)$ m, $R_y = (1000 \pm 170)$ m. The mean values show consistency in repeated measurements across several days for the same beam properties and optical setup. The total uncertainty includes the statistical uncertainty on the centroid fit, as well as the effect of event-to-event jitters in beam position.

A greater bending effect in the vertical plane is observed, consistent with a stronger field strength of the Earth's magnetic field in the horizontal plane measured in the experimental cavern [26]. Further analysis techniques and different measurement setups are under consideration to reduce uncertainties.

Orthogonal steering, as described [28], is used to align the electron beam for injection. This makes use of the last two corrector magnets on the line prior to the entrance aperture and is based on the kick-displacement response of the electron beam measured on the last two BTVs (3 and 4), in the inevitable presence of the Earth's magnetic field. Prior to each position adjustment, the two corrector magnets used are de-gaussed to avoid stray field effects. For more details on the procedure, see [28].

4.2. Vapour source heating system effects

Over the first 4.25 m, the AWAKE Run 2b vapour source is heated by electrical elements. These must be located inside of the vapour source μ-metal shielding for technical reasons. Their magnetic field effect on the electron bunch trajectory was investigated.

In order to measure this effect the electron bunch is aligned on axis (on the proton beam trajectory) and horizontally off axis in such a way that it travels, in vacuum, through the 10 m long vapour source. The electron bunch is imaged on two BTVs; one located prior to the entrance aperture (BTV4), the second located $\sim$2 m after the exit aperture (BTV5), see Fig. 1.

As expected, when turning the heaters on and off, the electron bunch centroid position was found to be constant (below the beam position jitters) on all BTVs upstream of the vapour source entrance. However, downstream of the vapour source exit, on BTV5, a significant (above beam position jitters) spatial displacement was observed.

In order to avoid the heating system from having any effect on electron beam trajectory inside the vapour source, all heaters are turned off 1 s before the arrival of the beams and for the duration of their propagation.

Recent tests found additional position deviations after the electron bunch enters the vapour source. These are constant in time, unrelated to the electrical elements and are currently under investigation.

4.3. Electron beam optics

The electron bunch is set to cross the wakefields at a given location z_e inside the vapour source. In reality however, due to the transverse extent of both the electron bunch and the plasma column ($\simeq$1 mm radius), the two will interact prior to z_e. The transverse extent of the wakefields is on the order of one plasma skin depth c/ω_{pe}, which ranges from c/ω_{pe}=167 to 529 μm for plasma electron densities used in AWAKE.

Due to aforementioned unavailability of diagnostics inside the vapour source, it is currently not possible to measure the transverse beam size at the location of injection. However, using the BTVs shown on Fig. 1, upstream measurements of the transverse beam size can be made.

On Fig. 2a, a measurement of the transverse electron beam distribution (measured using BTV4) with its waist at the entrance aperture ($\sim$ 9 cm further downstream) is depicted. It is important to note that the scale is not equal. The imaged beam's tilt is associated to a tilt in the last horizontal dipole on the electron transfer line [18, 16], i.e. it is not perfectly horizontal. This feature was included in multi-particle tracking (MAD-X) simulations of the electron bunch [29].

Figures 2b and 2c show the corresponding vertical and horizontal projections (green solid lines). Black solid lines show the results of Gaussian fits to the projections. Beam position centroid positions μ_x, μ_y (obtained from the Gaussian fits) are shown with solid blue lines on Figs. 2b and 2c and represent the beam centroid position well. This method is used in Section 4.1, to determine R_x and R_y based on beam centroid position measurements.

Gaussian fits to the projections in Figures 2b and 2c give root mean square (rms) beam sizes of $\sigma_{x,y} = (500, 150)\,\mu$m. These sizes are shown by the dashed (σ) and solid (2σ) horizontal lines (see Figs. 2b and c). Vertical dotted black lines show the corresponding $\mu_{x/y} \pm \sigma_{x/y}$ and $\mu_{x/y} \pm 2\sigma_{x/y}$ position values. The FWHM sizes are $\mathrm{FWHM}_{x,y} \simeq (1200, 350)\,\mu$m, and since $\mathrm{FWHM} = 2\sqrt{2\ln 2}\sigma$, they are in good agreement with the Gaussian fits. Correspondingly, solid horizontal red lines (and associated vertical dotted black lines) indicate these on Figs. 2b and 2c. Based on the good agreement, Gaussian fits are used to determine beam centroid position and transverse sizes.

For good witness bunch capture, the transverse size of the witness would ideally be comparable to or smaller than the transverse extent of the wakefields. The electron beam waist is thus set and optimised to be at the location of injection. The two quadrupole triplets in the electron beam line are used to rematch the optics to achieve this for each crossing position. The complexity of the beam line makes it extremely sensitive to errors in beam momentum during setup [18]. This in turn leads to asymmetric beams. As a result, the electron beam optics are in the process of being optimised for each focal point prior to injection using the available diagnostics where possible.

5. Witness bunch injection location

5.1. Uncertainty on the crossing position z_e

For the AWAKE Run 2b experiments, electron bunches serve as probes to evaluate the average longitudinal accelerating gradient ($W_{\parallel,av}$). Accurate evaluation requires knowledge of z_e, as $W_{\parallel,av} = \Delta E/(L - z_e)$, with L the plasma length and ΔE the electron energy gain from acceleration in the plasma wakefields. In this Section, sources for the uncertainty (Δz_e) on z_e are discussed. To simplify the calculation transversely Gaussian electron bunch profiles and straight trajectories are assumed.

The electron bunch crosses the plasma column at a shallow angle θ_i, typically on the order of a few milli-radians (mrad). Assuming a plasma column radius r_p (typically $r_p \simeq 1$ mm), the electron bunch centroid enters the plasma column $z_{\mathrm{cen}} = r_p/\theta_i$ prior to z_e, due to the transverse extent of the plasma. Specifically, $z_{\mathrm{cen}} \leq z_e$. For example, if $r_p = 1$ mm and $\theta_i = 2$ mrad, the bunch centroid enters the plasma column 0.5 m upstream of z_e. When combining

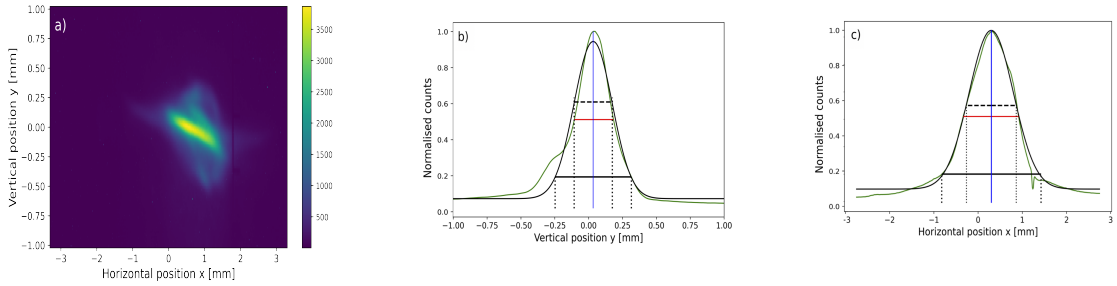

Figure 2. a) Example of a time-integrated electron bunch imaged on BTV4 for centroid determination and beamsize. Beam shape horizontally elongated. Scale not equal. b) Horizontal projection and fit of the measured beam in a). c) Vertical projection and fit of the measured beam in a).

the electron beam position jitter (below (50, 40) μm) with that of the laser pulse (position jitter $\sim 200\,\mu$m in both x and y), the uncertainty on the centroid crossing position between the two is $\Delta z_{\rm cen}^{plasma} = 0.082\,$m. Similarly, by combining the electron beam position jitter with the proton beam position jitter ($\sim 30\,\mu$m in both x and y) one obtains an uncertainty in centroid crossing position of $\Delta z_{\rm cen}^{wakefields} = 0.023\,$m.

The projected $\pm 2\sigma$ electron transverse beam size at the plasma column boundary provides a first estimate over which z-distance electrons enter the plasma column. The electron bunch size projected onto the plasma boundary (rather than the transverse extent of the wakefields) is taken as an estimate of the uncertainty. This is considered a reasonable yet conservative estimate, as beam evolution inside of the plasma column may be challenging to predict.

The projected electron bunch size at the plasma column (σ_{pc}) can be estimated from $\sigma_{pc} = \sigma_w \sqrt{1 + (z_{\rm cen}/\beta^*)^2}/\sin\theta_i$, where σ_w is the electron beam transverse size at the waist, and β^* is the electron beam beta function at the waist. For example, for $\sigma_w = 500\,\mu$m, $z_{\rm cen} = 0.5\,$m, $\beta^* = 0.5\,$m and $\theta_i = 2\,$mrad, then $\sigma_{pc} = 0.35\,$m. Adding this to z_{cen} one obtains $\Delta z_e = 0.85\,$m.

These simple estimates show that the smaller θ_i or the larger r_p, the larger $z_{\rm cen}$. This is important as bunch evolution inside of the plasma column may be very different from vacuum propagation. Additionally, smaller θ_i lead to larger σ_{pc}, further increasing uncertainty on the injection location. This is important, as typically only a very small fraction of the injected electron bunch is captured by and accelerated in the wakefields.

Beam and laser pulse position jitters further increase the uncertainty on z_e. However, their contributions (Δz_{cen}^{plasma} and $\Delta z_{cen}^{wakefields}$) are one order of magnitude lower than σ_{pc}. This underlines once more the strong dependence of the accuracy of injection location on the finite electron bunch size and θ_i.

5.2. Plasma-light diagnostic

A novel technique based on the electron bunch interaction with the plasma column was developed. When the electron bunch enters the plasma, it drives wakefields by depositing a part of its energy, some of which results in the emission of plasma-light [26, 30]. This light is emitted when plasma electrons are excited in neutral atoms or recombine with rubidium ions. The emitted light can be imaged on the digital cameras installed at the view-ports of the vapour source. The location where additional light is emitted is captured by the corresponding camera (as compared to the recombination light alone) and this in turn can be used to confirm the crossing of the electron bunch with the plasma column. This is important because there is no diagnostics inside of the vapour source and accurate beam steering is challenging (see

Section 4.1).

First plasma-light measurements illustrating this technique are shown in Fig. 3. For proof of principle, in these measurements the electron bunch (of high 800 pC charge) was aligned on the proton bunch trajectory (which is also the laser pulse trajectory) and its focus was set to be at the entrance aperture. No protons were present.

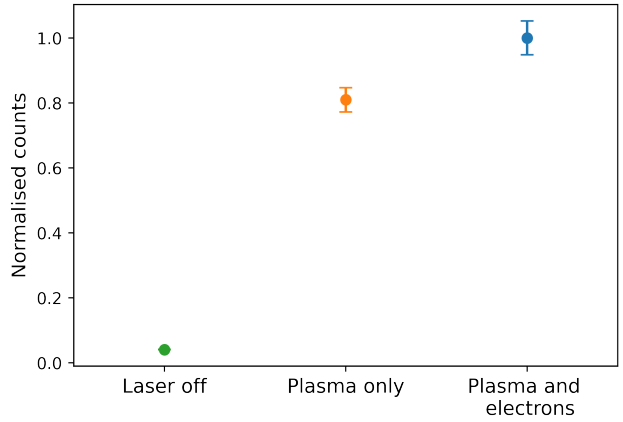

Figure 3. Detected plasma-light signal for background (Laser off), lowest point (green); plasma only (laser on, no electron beam), middle point (orange); and plasma and electrons (laser on and electron beam present), highest point (blue). All values are averaged and normalised. Uncertainties indicate full standard deviations.

Figure 3 shows that when the electron bunch propagates along the plasma column, a measurable light yield can be detected on the camera located at the first viewport ($z \sim 0.5$ m downstream of the vapour source entrance).

The green point on Fig. 3 ('Laser off') shows the detected camera background signal (summed counts, normalised to the peak value) when there is vapour, but no plasma (no laser pulse). The signal yield of this point is independent of the presence of the electron bunch. The orange point ('Plasma only') shows the same measurement for when there is plasma (rubidium vapour and laser pulse), but no electron beam. The average signal on the normalised scale is (0.81 ± 0.04). The blue point ('Plasma and electrons') shows a higher signal yield, measured for when the electron bunch is also present. The average signal on the normalised scale is (1.0 ± 0.05).

Numerical simulations predict that the electron bunch has to evolve (focus) before additional plasma-light signals become detectable. From the measurements shown on Fig. 3, it is clear that if the bunch has to first increase its density, $z \sim 0.5$ m is a sufficiently long evolution distance (for this bunch and focusing optics). This is consistent with the theoretical expectations which describe fast pinching of the electron bunch followed by strong wakefield driving within the first meter of interaction with plasma [31]. In the above described measurement configuration, additional plasma-light is observed until camera $z = 6.5$ m. The electron bunch is therefore driving sufficiently large (to be detected with plasma-light) wakefield amplitudes over a minimum distance of 6.5 m.

Excess plasma-light may therefore provide direct feedback on where electron bunches interact with the plasma column. This is especially useful when bunches are injected from the side (i.e. co-linearly with the wakefields in the vertical plane and crossing them at z_e in the horizontal plane). Observation of additional plasma-light signal does however not imply that the electron bunch trajectory is also crossing the wakefields (radius $\sim c/\omega_{pe}$), located inside of the plasma column. Small adjustments to the electron bunch trajectory may therefore be necessary once injection experiments are performed. However, images also show where the plasma and the proton bunch is. Their locations can be compared with the light signal location from the electrons to ensure spatial (average) overlap.

One notes that the rough estimate on the uncertainty of the crossing location of the electron

bunch with the plasma column, is comparable to the spacing between view ports (1 m) of the vapour source, giving an upper bound on the possible z_e accuracy of this method.

6. Summary and Outlook

In this manuscript, the AWAKE Run 2b external, off-axis witness (electron) bunch injection setup is described. Successful injection leads to electron acceleration and allows to measure energy gain. Energy gain, when divided by the acceleration length, provides the average longitudinal wakefield amplitude and allows the study of the plasma density step's effectiveness.

It is highlighted that the new racetrack shape of the vapour source entrance aperture allows for larger witness injection angles. Larger injection angles up to a few milli-radians (limited also by the experimental setup) are favorable as they decrease injection location uncertainties and were shown to improve charge capture in numerical simulations.

Measures to minimize differences between the calculated and observed electron beam trajectories prior to the entrance aperture were implemented. Firstly, the presence of the Earth's magnetic field was identified and quantified via its resulting effect of beam centroid displacements. These are accounted for by trajectory corrections provided by corrector magnets and automatic steering. Secondly, unwanted steering caused by the fields generated by the electric vapour source heaters was mitigated by turning them off during beam propagation.

Accurate determination of the average longitudinal wakefield amplitude requires knowledge on the acceleration length. Since the plasma is 10 m long, it can be obtained from subtracting the location where electrons are injected into the wakefields from the plasma length. It is shown that digital cameras capturing plasma-light (created by energy deposition of the witness bunch) provide feedback on where and when electrons interact with the plasma column. The injection location uncertainty due to finite electron bunch and plasma column size is estimated to be on the meter scale for an injection angle $\theta_i = 2$ mrad. This uncertainty decreases for larger injection angles.

As a next step, off axis injection experiments using plasma-light to confirm crossing location are planned. To reduce uncertainties on beam optics, dedicated comparisons of measured and simulated electron beam transverse distributions are also under way. These results are an important step and necessary studies to realise electron injection for AWAKE Run 2b, scheduled for 2024.

References

[1] Turner M, Bracco C, Gessner S, Goddard B, Gschwendtner, Muggli P, Asmus F P, Velotti F and Verra L 2018 *Proc. Adv. Acc. Conf.* (Colorado: USA) pp 1-4
[2] Schroeder CB, Benedetti C, Esarey E, Grüner FJ and Leemans WP 2011 Growth and Phase Velocity of Self-Modulated Beam-Driven Plasma Waves *Phys. Rev. Lett.* **107** 145002
[3] Kumar N, Pukhov A and Lotov KV 2010 Self-Modulation Instability of a Long Proton Bunch in Plasmas *Phys. Rev. Lett.* **104** 255003
[4] Demeter G, Moody JT, Kedves MÁ, Batsch F, Bergamaschi M, Fedosseev V, Granados E, Muggli P, Panuganti H and Zevi Della Porta, G 2024 Generation of 10-m-lengthscale plasma columns by resonant and off-resonant laser pulses *Optics and Laser Technology* **168** p.109921
[5] Fedosseev V et al 2016 *Proc. Int. Part. Acc. Conf. (IPAC'16)* (Busan: Korea)
[6] Lotov KV, Lotova GZ, Lotov VI, Upadhyay A, Tückmantel T, Pukhov A and Caldwell A 2013 Natural noise and external wakefield seeding in a proton-driven plasma accelerator *Phys. Rev. Sp. Top. Accelerators and Beams* **16** 041301
[7] Batsch F et al (AWAKE Collaboration) 2021 Transition between Instability and Seeded Self-Modulation of a Relativistic Particle Bunch in Plasma *Phys. Rev. Lett.* **126** 164802
[8] Turner M et al (AWAKE Collaboration) 2019 Experimental Observation of Plasma Wakefield Growth Driven by the Seeded Self-Modulation of a Proton Bunch *Phys. Rev. Lett.* **122** 054801
[9] Adli E et al (AWAKE Collaboration) 2019 Experimental Observation of Proton Bunch Modulation in a Plasma at Varying Plasma Densities *Phys. Rev. Lett.* **122** 054802

[10] Adli E et al (AWAKE Collaboration) 2018 Acceleration of electrons in the plasma wakefield of a proton bunch *Nature* **561** 363-7
[11] Lotov KV 2015 Physics of beam self-modulation in plasma wakefield accelerators *Phys. Plasmas* **22** 103110
[12] Gschwendtner E et al (AWAKE Collaboration) 2022 The awake run 2 programme and beyond *Symmetry* **14** 1680
[13] Muggli P, Bergamaschi M, Pucek J, Easton D, Pisani J and Uncles J 2022 *Proc. Adv. Acc. Conf.* (Long Island, NY: USA)
[14] Kim Y et al 2020 Commissioning of the electron injector for the AWAKE experiment *Nucl. Instrum. Meth. in Phy. Res.* A **953** 163194
[15] Pepitone K et al 2018 The electron accelerators for the AWAKE experiment at CERN baseline and future developments *Nucl. Instrum. Meth.* A **909** pp 102-6
[16] Schmidt JS et al 2016 Status of the proton and electron transfer lines for the AWAKE Experiment at CERN *Nucl. Instrum. Meth.* A **829** pp 58-62
[17] Velotti FM, Goddard B, Kain V, Ramjiawan R, Della Porta GZ, Hirlaender S 2023 Towards automatic setup of 18 MeV electron beamline using machine learning *Machine Learning: Science and Technology* **4(2)**025016
[18] Bracco C et al 2019 *Proc. Int. Part. Acc. Conf. (IPAC'19)* (Melbourne: Australia) p 2383
[19] Mazzoni S et al 2017 *Proc. Int. Part. Acc. Conf. (IPAC'17)* (Copenhagen: Denmark) p 404
[20] Schroeder CB, Benedetti C, Esarey E, Grner FJ, and Leemans WP 2011 Growth and phase velocity of self-modulated beam-driven plasma waves *Phys. Rev. Lett.* **107** 145002
[21] Lotov KV et al 2014 Electron trapping and acceleration by the plasma wakefield of a self-modulating proton beam *Phys. Plasmas* **21** 123116
[22] Lotov KV 2012 Optimum angle for side injection of electrons into linear plasma wakefields *J. Pla. Phys.* **78** pp 455-9
[23] Pukhov A, Kumar N, Tückmantel T, Upadhyay A, Lotov KV, Muggli P, Khudik V, Siemon C and Shvets G 2011 Phase Velocity and Particle Injection in a Self-Modulated Proton-Driven Plasma Wakefield Accelerator *Phys. Rev. Lett.* **107** 145003
[24] Pakuza C et al *Proc. Int. Part. Acc. Conf. (IPAC'23)* (Venice: Italy) pp 4806-9
[25] Plyushchev G et al 2018 *J. Phys. D: Appl. Phys.* **51** 025203
[26] Verra L et al (AWAKE Collaboration) 2022 Controlled growth of the self-modulation of a relativistic proton bunch in plasma *Phys. Rev. Lett.* **129** 024802-7
[27] Verra L et al 2020 Electron beam characterization with beam loss monitors *Phys. Rev. Acc. Beams* **23** 032803-6
[28] Bencini V, Doebert S, Gschwendtner E, Granados E, Velotti FM, Verra L and Zevi Della Porta G 2023 *Proc. Int. Part. Acc. Conf. (IPAC'23)*, (Venice: Italy) pp 291-4
[29] MAD-X PTC Multi-particle tracking http://mad.web.cern.ch/mad/
[30] Oz E et al 2004 *Proc. Adv. Acc. Conf.*(Stony Brook, New York: USA) vol 737 pp 708–14
[31] Zevi Della Porta G et al *Proc. Int. Part. Acc. Conf. (IPAC'21)* (Campinas, SP: Brazil) pp 1761-4